Hierarchical Representation and Simulation of Micromachined Inertial Sensors

Jan E. Vandemeer, Michael S. Kranz, Gary K. Fedder*

Department of Electrical and Computer Engineering, and *The Robotics Institute
Carnegie Mellon University, Pittsburgh, Pennsylvania 15213-3890
Telephone: (412) 268-4275 Fax: (412) 268-2860 E-mail: jev@ece.cmu.edu

ABSTRACT

A circuit-level methodology for simulating micromachined inertial sensors based on a hierarchical representation of microelectromechanical systems (MEMS) is presented. In the NODAS methodology (NOdal Design of Actuators and Sensors), microaccelerometers and microgyroscopes are designed as netlists of general-purpose micromechanical beams, plates, electrostatic gaps, joints, and anchors and evaluated using lumped-parameter behavioral models. The on-chip displacements and global position of each micromechanical element have been separated in the netlist, enabling application of translation and rotation of the chip while simultaneously providing access to on-chip displacements for position sensing and electrostatic actuation. Simulations of static displacements and modal frequencies of a cantilever beam, a crab-leg accelerometer, and a symmetric vibratory-rate gyroscope agree to within 2% of finite-element analysis when using the minimal number of elements. Simulation of a 16 kHz vibratory-rate gyroscope system with dual transresistance sense amplifiers illustrates the ability to perform system-level mixed-domain simulation.

Keywords: nodal simulation, lumped-parameter modeling, inertial sensors.

I. INTRODUCTION

The increasing integration of microelectromechanical systems (MEMS) has heightened the demand for computer-aided design (CAD) tools to support rapid design of systems involving interactions between physical energy domains. An important subset of MEMS are suspended electromechanical structures, such as resonant sensors, accelerometers, and vibratory-rate gyroscopes. We describe continuing work on a hierarchical MEMS representation and an associated mixed-domain nodal simulation for rapid design and evaluation of suspended MEMS.

Most previous work on MEMS behavioral simulation has focused on first forming reduced-order macromodels of devices (e.g., resonators, hot plates) using finite-element or boundary-element simulation [1][2]. Several groups are attempting to automate the macromodel extraction procedure. This approach is suitable for evaluation of existing devices, but it inhibits a top-down design flow for new devices.

More recently, work has been done by Pister [3][4] and the authors [5] on developing "circuit-level" design tools for suspended MEMS based on a hierarchical decomposition of suspended MEMS into a handful of reusable elements: beams, plates, electrostatic gaps, beam joints, and anchors. Using this representation, elements can be interconnected in a general way to design complex MEMS. The lumped-parameter element models are reusable and can be upgraded without altering the device netlist. The hierarchical representation, called NODAS for NOdal Design of Actuators and Sensors, is currently implemented in the Saber simulator with models written in MAST, an analog hardware description language [6]. Presently, the implementation is restricted to simulation of in-plane motion (x, y, θ), with coupled electrostatic and electrical effects.

In this paper, a second generation of MEMS hierarchical components are described. The instantaneous position of each element in the design (i.e., on the chip) is separated into two sets of nodes. A zero-force position (X, Y, Θ) relative to an external (global) frame of reference is modified by rigid-body translation and rotation of the chip. Displacement relative to the chip (x, y, θ) results from any forces acting on the elements. Inertial forces from external motion of the chip and from on-chip acceleration are incorporated into the element models to accurately reflect the behavior of microaccelerometers and microgyroscopes.

The remainder of the paper describes the theory of the MEMS schematic and nodal simulation, followed by a verification with finite-element analysis using examples of a crab-leg flexure, a crab-leg accelerometer, and a vibratory-rate gyroscope.

II.DESCRIPTION OF NODAL SIMULATION

Static equilibrium dictates that the forces acting on a body must sum to zero. Likewise the sum of moments must also equal zero. These equations are called the "through" variable relations, and are analogous to Kirchoff's Current Law in circuit theory. Nodal simulators solve for system variables by making the sum of the "through variables" flowing out of each node equal to zero. By defining component models (templates) using an Analog Hardware Description Language (A-HDL), one can create equations which relate the multi-domain through variables in terms of the across variables. In the NODAS methodology, the through variables are forces in x and y, moments in θ, and electrical current; the across variables are translational displacements in x and y, rotational displacements in θ, and voltage. The simulator solves for the across variables within each template, and then solves equations involving through variables via substitution. A

positive value of a force through variable when entering a node is interpreted as a force along the positive axis acting on the element at that node. A positive value of a torque through variable is interpreted as a torque rotated in a counterclockwise direction about the z-axis acting on the element at that node.

MEMS elements have a certain physical size and orientation associated with them. For example, a micromechanical beam has a length, width, and angle which is represented by the schematic element shown in Figure 1. Beam thickness and material properties are considered part of the process and are set in a separate technology file. These user-defined values are incorporated into the behavioral model of the beam. For example, in a crab-leg flexure (Figure 2) when a horizontal beam is placed into a schematic, its left (or minus) side has a certain rest position (x, y, θ), and its right (or plus) side has the position (x + length, y, θ). The position of a vertical beam is oriented lengthwise from bottom to top (+y direction).

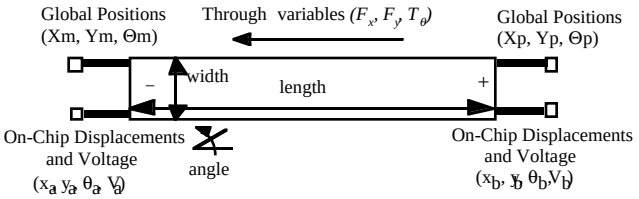

Figure 1. Beam element, showing global position nodes (X, Y, Θ), and on-chip displacement nodes (x, y, θ).

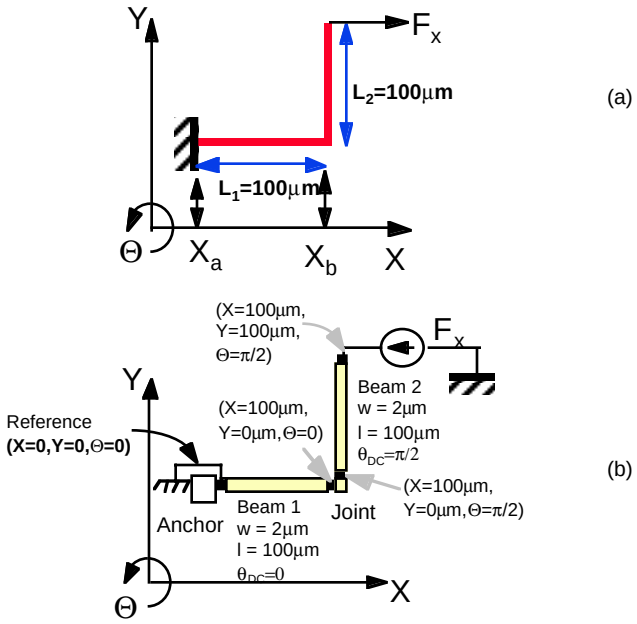

Figure 2. (a) Layout view of crab-leg flexure, (b) Schematic view of crab-leg flexure.

III. THEORY

Forces and displacements in the chip frame of reference for a specific element are expressed as vectors **F** and **u** respectively. In the case of the beam element, there are two ports, a and b (or + and -), corresponding to the two sides of the beam.

$$\mathbf{F} = \begin{bmatrix} F_{xa} & F_{ya} & \tau_{\theta a} & F_{xb} & F_{yb} & \tau_{\theta b} \end{bmatrix}^T \quad (1)$$

$$\mathbf{u} = \begin{bmatrix} x_a & y_a & \theta_a & x_b & y_b & \theta_b \end{bmatrix}^T \quad (2)$$

The beam displacements are transformed into the local frame of reference of the beam, yielding the local displacement,

$$\mathbf{u_L} = \Omega_L^{-1} \cdot \mathbf{u} \quad (3)$$

where Ω_L is the local rotation matrix given by

$$\Omega_L = \begin{bmatrix} \cos\theta_{DC} & -\sin\theta_{DC} & 0 & 0 & 0 & 0 \\ \sin\theta_{DC} & \cos\theta_{DC} & 0 & 0 & 0 & 0 \\ 0 & 0 & 1 & 0 & 0 & 0 \\ 0 & 0 & 0 & \cos\theta_{DC} & -\sin\theta_{DC} & 0 \\ 0 & 0 & 0 & \sin\theta_{DC} & \cos\theta_{DC} & 0 \\ 0 & 0 & 0 & 0 & 0 & 1 \end{bmatrix} \quad (4)$$

and θ_{DC} is the angle at which the beam is oriented in its zero-force state (for an example, refer to Figure 2). Small angle approximations are made in modeling the beam element. Forces and moments in the local frame of reference are solved using the element stiffness matrix, **k**.

$$\mathbf{k} = \frac{EI_z}{L^3} \begin{bmatrix} \frac{AL^2}{I_z} & 0 & 0 & -\frac{AL^2}{I_z} & 0 & 0 \\ 0 & 12 & 6L & 0 & -12 & 6L \\ 0 & 6L & 4L^2 & 0 & -6L & 2L^2 \\ -\frac{AL^2}{I_z} & 0 & 0 & \frac{AL^2}{I_z} & 0 & 0 \\ 0 & -12 & -6L & 0 & 12 & -6L \\ 0 & 6L & 2L^2 & 0 & -6L & 4L^2 \end{bmatrix} \quad (5)$$

as described by Przemieniecki in [7]. In these matrices, E is Youngs modulus, A is the cross sectional area of the beam, and I_z is the moment of inertia of the beam about the z-axis. The local forces are then transformed back into the chip frame of reference, resulting in the through variables of force.

$$\mathbf{F} = -\Omega_L \cdot \mathbf{k} \cdot \Omega_L^{-1} \cdot \mathbf{u} \quad (6)$$

Effective mass is included in the beam by solving for the equivalent element mass matrix **m** of a uniform beam and multiplying by the local accelerations $\Omega_L^{-1}\ddot{\mathbf{u}}$ at the ends of the beam. The inertial forces in the local frame are then transformed back into the chip frame, yielding:

$$\mathbf{F} = -\Omega_L \cdot \mathbf{m} \cdot \Omega_L^{-1} \cdot \ddot{\mathbf{u}} \quad (7)$$

To solve for the mass matrix, a matrix, **a**, of shape functions is defined, which relates the distributed displacement of the beam to the nodal displacements in the local frame [7].

$$\mathbf{y_L(x) = a^T u_L} \tag{8}$$

Assuming a static mode shape across the beam, and neglecting rotary inertia and shear deformation, the shape functions are:

$$\mathbf{a} = \begin{bmatrix} 1 - \frac{\xi}{L} \\ 1 + \frac{2\xi^3}{L^3} - \frac{3\xi^2}{L^2} \\ \xi + \frac{\xi^3}{L^2} - \frac{2\xi^2}{L} \\ \frac{\xi}{L} \\ \frac{3\xi^2}{L^2} - \frac{2\xi^3}{L^3} \\ \frac{\xi^3}{L^2} - \frac{\xi^2}{L} \end{bmatrix} \tag{9}$$

where ξ represents the position along the length of the beam. From principles of virtual work, the mass matrix is [7]:

$$\mathbf{m} = \int_0^L \rho \mathbf{A a^T a} d\xi \tag{10}$$

where ρ is the material density of the beam. The nodal mass matrix is:

$$\mathbf{m} = -\frac{\rho AL}{420}\begin{bmatrix} 140 & 0 & 0 & 70 & 0 & 0 \\ 0 & 156 & 22L & 0 & 54 & -13L \\ 0 & 22L & 4L^2 & 0 & 13L & -3L^2 \\ 70 & 0 & 0 & 140 & 0 & 0 \\ 0 & 54 & 13L & 0 & 156 & -22L \\ 0 & -13L & -3L^2 & 0 & -22L & 4L^2 \end{bmatrix} \tag{11}$$

The inertial force and torque is then inserted at the appropriate nodes at the endpoints of the beam as shown in Figure 3.

For simulation of inertial sensors, it is necessary to include the global inertial effects on the on-chip

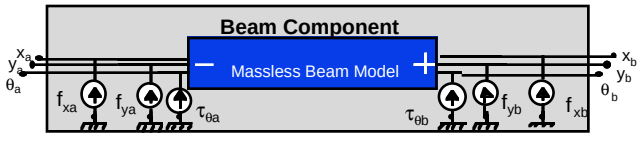

Figure 3. The beam component with equivalent forces due to effective mass. The position across variables are not shown.

displacements. Currently, inertial effects from both external and on-chip motion are included in the plate-mass component model. All motions are referred to the global frame of reference to calculate the inertial force, which gives rise to Coriolis effects and centrifugal forces in the chip frame of reference.

Generation of inertial forces for each element is accomplished by transforming the on-chip displacement $\mathbf{x_c}$ into the global frame through the global rotation matrix Ω_g, solving for the accelerations, and adding them to the global external accelerations $d^2\mathbf{X_g}/dt^2$. The total acceleration is then transformed back into the chip frame of reference through the inverse of the global rotation matrix Ω_g, and multiplied by the mass ($\rho\mathbf{AL}$) to determine the inertial force acting on the plate ($\mathbf{F_i}$).

$$\mathbf{F_i} = (\rho \mathbf{AL})\Omega_g^{-1}\left(\ddot{\mathbf{X}}_g + (\ddot{\Omega_g \mathbf{x}_c})\right) \tag{12}$$

The global rotation matrix is given by:

$$\Omega_g = \begin{bmatrix} \cos\Theta & -\sin\Theta & 0 & 0 & 0 & 0 \\ \sin\Theta & \cos\Theta & 0 & 0 & 0 & 0 \\ 0 & 0 & 1 & 0 & 0 & 0 \\ 0 & 0 & 0 & \cos\Theta & -\sin\Theta & 0 \\ 0 & 0 & 0 & \sin\Theta & \cos\Theta & 0 \\ 0 & 0 & 0 & 0 & 0 & 1 \end{bmatrix} \tag{13}$$

where Θ represents the angle of the component with respect to the global coordinate system.

Electrostatic actuators may be modeled as combinations of beams and electrostatic gaps. However, for the simulations in this paper, we use a simple first-order macromodel of the electrostatic comb-finger actuator [12].

IV. SIMULATION

The NODAS hierarchical representation and nodal simulation has been implemented in SABER [8] with the lumped models written in the MAST hardware description language. Force-displacement relations of the crab-leg flexure shown in Figure 2 were simulated and compared to finite element simulation (ABAQUS [9]) to demonstrate accuracy. In Figure 4, displacement of the end of the flexure in x and y are plotted as a function of applied force in x. The NODAS and ABAQUS results match to better than 1% for small deflections where the beam spring constant is linear. As expected, the error increases as the spring force becomes nonlinear.

Accuracy of the steady-state ac analysis is demonstrated with the crab-leg accelerometer shown in Figure 5(a). The corresponding MEMS schematic in Figure 5(b) consists of a plate mass suspended by crab-leg flexures made from beam components. Comb drives are placed on the left and right side of the plate-mass to sense x-axis motion differentially. Transresistance amplifiers are placed at the outputs of the comb drives to sense motional current.

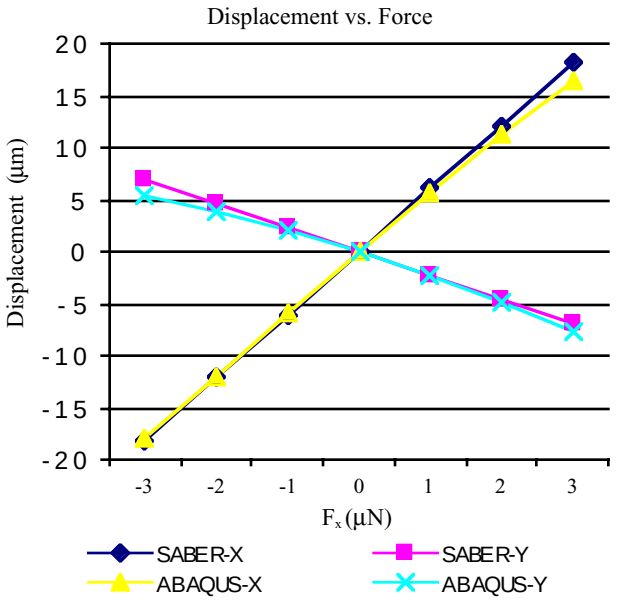

Figure 4. Graph of force versus displacement for a crab-leg flexure.

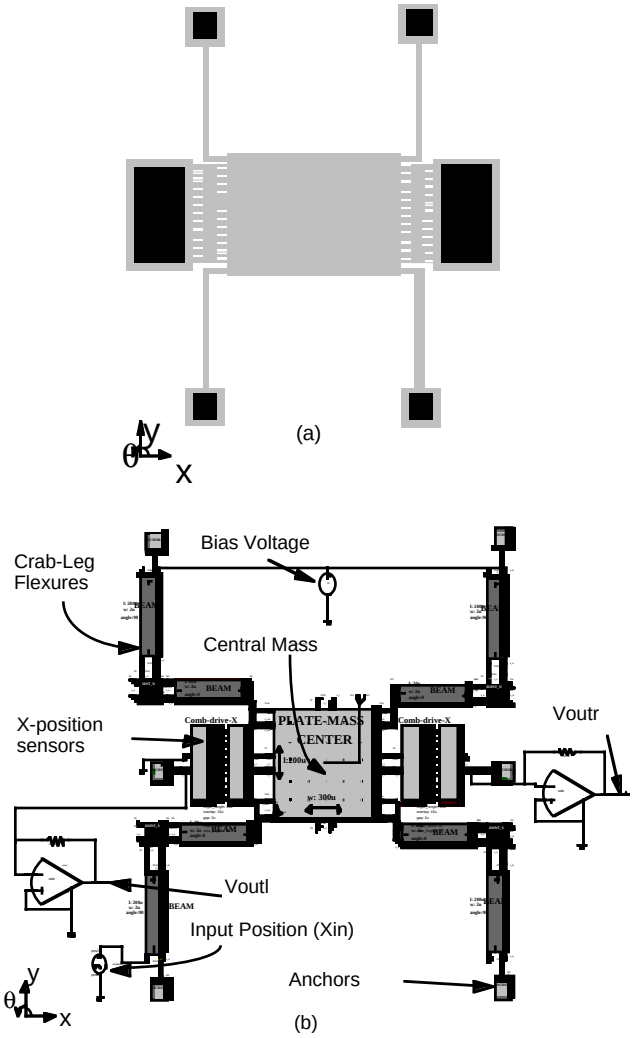

Figure 5. Crab-leg accelerometer (a) Layout view, (b) Schematic view.

A sinusoidal position source, X_{in}, with amplitude 1nm and frequency ω_c, drives one of the X_g in the global frame of reference to emulate an external lateral motion of the chip. The motion corresponds to an external acceleration of amplitude $(1nm)\omega_c^2$ and gives the transfer function of the system a high pass characteristic.

$$\mathbf{X_{out}}(\omega_c) = X_{in}\frac{\mathbf{m}\omega_c^{\,2}}{\sqrt{1-\left(\frac{\mathbf{m}\omega_c^{\,2}}{\mathbf{k}}\right)^2+\left(\frac{\mathbf{B}\omega_c}{\mathbf{k}}\right)^2}} \qquad (14)$$

where m represents the effective mass of the system, B is the damping coefficient, and k is the effective spring constant. The ac analysis results in Figure 6 display a resonant frequency of 10.24 kHz. The resonant frequency was calculated as 10.39 kHz using analytical equations, and as 10.38 kHz by using finite element methods. These values match to within 2%. The quality factor in air of 34.3 was calculated via analytical equations, which is within 2% of the quality factor of 33.8 measured with SABER.

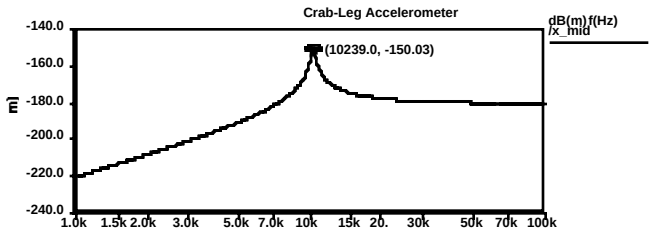

Figure 6. AC Analysis on crab-leg accelerometer.

Next, a vibratory-rate gyroscope was simulated to demonstrate the ability to analyze relatively complex inertial microsystems using NODAS. The vibratory rate gyroscope shown in Figure 7 consists of a system of beams and masses which are designed with three-fold symmetry to match mechanical modes in the x and y directions [10]. The gyroscope uses these two degrees of motion to detect rotation. One direction (in this case, x) is chosen to be the direction in which the gyroscope is actuated. It is actuated at the resonant frequency of the system to maximize displacements and increase sensitivity. External rotation about the z axis generates a Coriolis force acting in the y direction that is proportional to rotational rate.

An equivalent schematic of the vibratory rate gyroscope, shown in Figure 8, was created using the beam, plate, joint, anchor, and comb-drive components from a library. The entire movable structure is connected to a dc bias source. Differential electrostatic comb drives are located in both the x axis and y axis. The left-hand x-axis comb actuator is driven with an ac input voltage (v_drive) that operates at the mechanical resonant frequency. The right-hand x-axis comb in conjunction with a transresistance amplifier is used to detect the sinusoidal drive velocity. This signal is then used to demodulate the differential output signal.

The comb drives and transresistance amplifiers mounted on the y axis sense motion due to the Coriolis

force. An angle source (PHIin) in the global frame of reference was attached at the center of mass of the system to simulate external rotation of the chip.

To verify the accuracy of the mechanical models, an ac analysis was first performed with NODAS and compared to a modal analysis done with finite elements. As shown in Table 1, the analyses match to within 1.5%. The symmetry of the design is also shown in the ac analysis by the equivalence of the x and y resonant modes (16.23kHz).

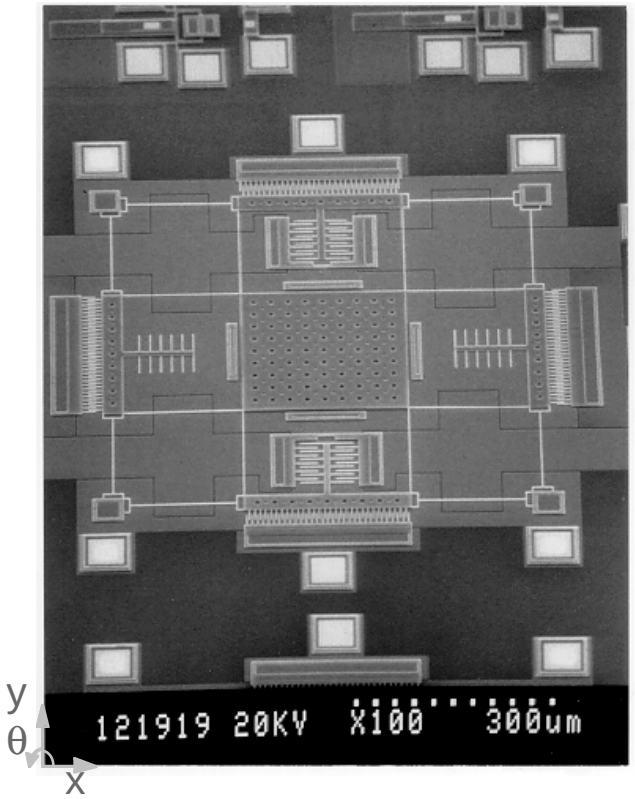

Figure 7. Scanning electron microscope of a three-fold symmetric vibratory-rate gyroscope fabricated in the MCNC MUMPs process [11].

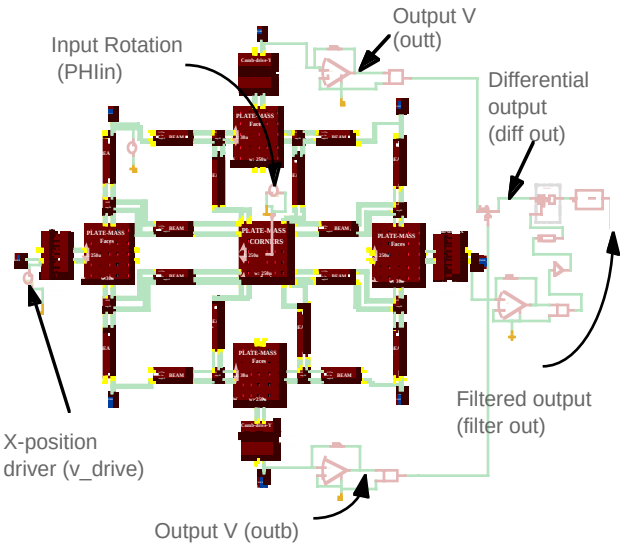

Figure 8. Equivalent schematic view of the vibratory-rate gyroscope.

A transient analysis of the gyroscope is shown in Figure 9 and Figure 10. The x-axis drive voltage (v_drive) was assigned an amplitude of 5 V p-p and a frequency of 16.23kHz. The external angle source (PHIin) was set to rotate the chip with an amplitude of 1 radian at a frequency of 50 Hz. A 40 V dc bias was set on the movable structure to enable a motional current in the y-axis comb sensors. Figure shows the envelope of the x-axis motion of the system caused by the sinusoidal input drive voltage.

When the input rotation (PHIin) is applied (Figure 10(a)), motional current in the y direction arising from the Coriolis force is sensed by the upper and lower transresistance amplifiers, as seen in the output voltage in Figure 10(b). In order to eliminate common mode disturbances, the difference of the top and bottom

	NODAS	*ABAQUS (FEA)*
ω_{rx} (Hz)	16.23k	16.00k
ω_{ry} (Hz)	16.23k	16.00k
$\omega_{r\theta}$ (Hz)	57.41k	57.1k

Table 1. Calculation of the first three modal frequencies of the three-fold symmetric gyroscope. Resonant frequency values match to within 1.5 %.

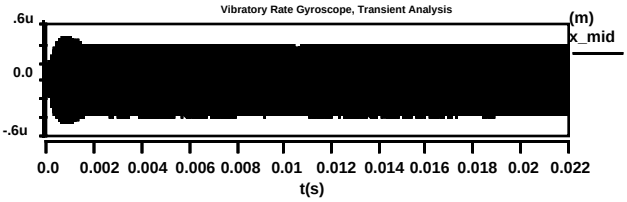

Figure 9. X-axis motion of the gyroscope caused from the input drive voltage (v_drive).

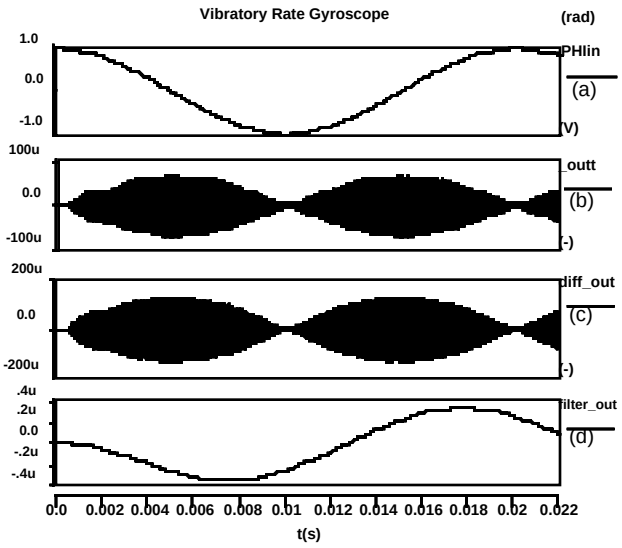

Figure 10. Gyroscope transient simulation waveforms. (a) External rotation applied at center of mass (PHIin), (b) Top y-axis amplifier voltage (outt), (c) Differential output voltage (diff_out) from subtraction of the upper comb signal from the lower comb signal, (d) Final demodulated and filtered output (filter_out).

output signals are computed and shown in Figure 10(c). Finally, this signal is demodulated with the electrical output from the drive signal (v_drive) and fed through a low-pass filter to eliminate the drive harmonics (Figure 10(d)). The phase shift in the final output is an artifact of the low-pass filter.

As is true of all simulation, NODAS has a speed vs. accuracy trade-off. Simulation time can be reduced by sacrificing the order of the models, and by using simpler models. Conversely, complex high-order effects can be simulated if one is willing to wait long enough.

One way the user can speed up their simulation is by using "level 1" models of the components (i.e., beams with no effective mass, or plates with no global inertial effects) in situations that are mainly independent on these effects. One example would be the vibratory rate gyroscope. The mass of the beams is rather small relative to the mass of the plates. If one replaces the beams that include effective mass with the massless beams, one can save large amounts of simulation time. It took approximately 32 minutes on a Sun Ultra-Sparc-2 workstation to simulate the vibratory rate gyroscope system when the beams included inertial effects. An equivalent simulation with massless beams completed in only 5 minutes, and provided a fundamental resonant frequency of 16.7 kHz (within 5% of finite element calculations). Simulation time can also be reduced by choosing various components that will provide the same functionality for fewer nodes. For example, one could replace all the anchors in a system by connecting each separate substrate contact to a single anchor component.

A simple cantilever beam experiment was performed to examine the relation between the number of beam components to simulation time. The simulation time of a transient analysis was recorded for a cantilever containing beams with and without effective mass. After each simulation, extra beam components were added on, while their lengths were modified to keep the sum of the lengths at 100µm. The results show that the simulation time increases linearly with the number of components in the case of the massless beams, while the increase is exponential for the beams with inertia (Figure 11).

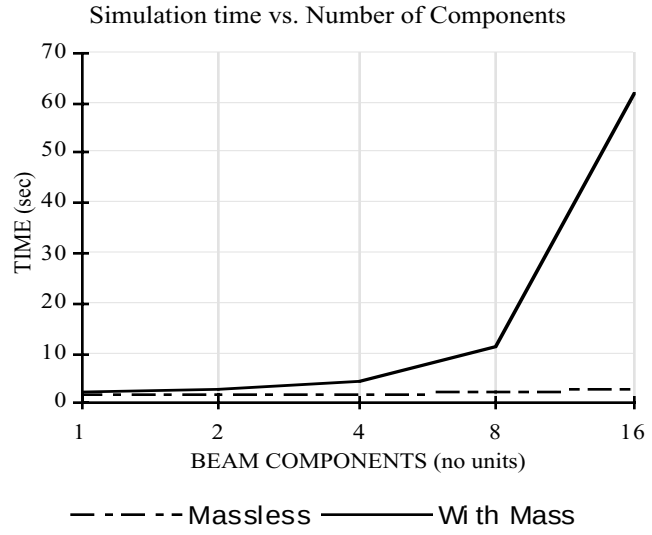

Figure 11. Execution time vs. number of beam elements for a cantilever beam transient analysis (1ms simulation time).

CONCLUSIONS

This paper describes a methodology for Nodal Design of Actuators and Sensors (NODAS) which uses a hierarchical representation of MEMS components implemented in an analog hardware description language and simulated with a nodal simulator. Using the NODAS design methodology will allow a designers to quickly and easily create complex MEMS designs and build up a hierarchical parts library for reuse in future designs.

The second-generation components described in this paper add much more flexibility and accuracy to designs. The inertial beams increase the accuracy of simulations. The global inertial forces included in the plate mass model enable test of inertial sensors. The addition of global inertial forces in the beams is left as future work. The ability to perform multi-domain simulation allows easy evaluation of integrated electronics or control systems with microelectromechanical devices.

ACKNOWLEDGEMENTS

This research effort is sponsored by an NSF CAREER Award; and by the Defense Advanced Research Projects Agency (DARPA) and U. S. Air Force Research Laboratory, under agreement number F30602-96-2-0304. The U. S. Government is authorized to reproduce and distribute reprints for governmental purposes not with standing any copyright notation thereon. The views and conclusions contained herein are those of the authors and should not be interpreted as necessarily representing the official policies or endorsements, either expressed or implied, of DARPA, the U. S. Air Force Research Laboratory, or the U. S. Government.

REFERENCES

[1] J.M. Karam, et.al., APCHDL '96, Bangalore, India, 8-10 January, 1996.

[2] J. Scholliers, et.al., Proc. IEEE Intl. Conference on Robotics and Automation, Nagoya, Japan, 21-27 May 1995, vol. 3, pp. 2847-52.

[3] E. C. Berg, et.al., ACM SIGDA Physical Design Workshop, Reston VA, April 1996, pp. 66-70.

[4] J. Clark, N. Zhou, S. Brown and K.S.J. Pister, "Nodal Analysis for MEMS Simulation and Design", MSM -98, Santa Clara, CA, 6-8 April, 1998.

[5] J. Vandemeer, et.al., ASME Winter Annual Conference, Dallas, TX, 16-21 November, 1997.

[6] MAST Reference Manual, Release 4.2, Analogy Inc., Beaverton OR, 1997.

[7] S. P. PrzemienieckiTheory of Matrix Structural Analysis", McGraw-Hill, New York, New York, 1968.

[8] SaberGuide and SaberScope Manual, Release 4.2, Analogy Inc., Beaverton OR, 1997.

[9] ABAQUS/Standard User's Manual, Version 5.6, Volume II, Hibbitt, Karlson and Sorenson Inc., Pawtucket RI, 1996.

[10] M. Kranz, G.K. Fedder "Micromechanical Vibratory Rate Gyroscopes Fabricated in Conventional CMOS", Symposium Gyro Technology 1997, Stuttgart, Germany, pp. 3.0-3.8.

[11] D. A. Koester, et. al., *Multi-User MEMS Processes (MUMPs) Introduction and Design Rules*, MCNC MEMS Technology Applications Center, 3021 Cornwallis Road, Research Traingle Park, NC 27709, rev. 3, Oct. 1994, 39 pages.

[12] W. C. Tang, T.-C. H. Nguyen, M. W. Judy, and R. T. Howe, "Electrostatic comb drive of lateral polyilicon resonators," *Sensors and Actuators* A, vol.2, no.1-3, pp. 328-31, Feb. 1990.